

Article

Anodic Stripping Voltammetric Analysis of Trace Arsenic(III) on a Au-Stained Au Nanoparticles/Pyridine/Carboxylated Multiwalled Carbon Nanotubes/Glassy Carbon Electrode

Yun Du ^{1,2} , Chenglong Sun ¹, Yuru Shen ¹, Luyao Liu ¹, Mingjian Chen ¹, Qingji Xie ^{1,*} and Hongbo Xiao ^{3,*}

¹ Key Laboratory of Chemical Biology & Traditional Chinese Medicine Research, Ministry of Education of China, College of Chemistry and Chemical Engineering, Hunan Normal University, Changsha 410081, China; hello_dudu1990@163.com (Y.D.); 15588654717@163.com (C.S.); shenyuru163@163.com (Y.S.); lly19970214@163.com (L.L.); mingjian412@163.com (M.C.)

² Changsha Center for Diseases Prevention and Control, Changsha 410004, China

³ College of Science, Central South University of Forestry and Technology, Changsha 410004, China

* Correspondence: xiejq@hunnu.edu.cn (Q.X.); anabeel@126.com (H.X.)

Abstract: A Au-stained Au nanoparticle (Au_s)/pyridine (Py)/carboxylated multiwalled carbon nanotubes (C-MWCNTs)/glassy carbon electrode (GCE) was prepared for the sensitive analysis of As(III) by cast-coating of C-MWCNTs on a GCE, electroreduction of 4-cyanopyridine (cPy) to Py, adsorption of gold nanoparticles (AuNPs), and gold staining. The Py/C-MWCNTs/GCE can provide abundant active surface sites for the stable loading of AuNPs and then the AuNPs-initiated Au staining in HAuCl₄ + NH₂OH solution, giving a large surface area of Au on the Au_s/Py/C-MWCNTs/GCE for the linear sweep anodic stripping voltammetry (LSASV) analysis of As(III). At a high potential-sweep rate of 5 V s⁻¹, sharp two-step oxidation peaks of As(0) to As(III) and As(III) to As(V) were obtained to realize the sensitive dual-signal detection of As(III). Under optimal conditions, the ASLSV peak currents for oxidation of As(0) to As(III) and of As(III) to As(V) are linear with a concentration of As(III) from 0.01 to 8 μM with a sensitivity of 0.741 mA μM⁻¹ and a limit of detection (LOD) of 3.3 nM (0.25 ppb) (*S/N* = 3), and from 0.01 to 8.0 μM with a sensitivity of 0.175 mA μM⁻¹ and an LOD of 16.7 nM (1.20 ppb) (*S/N* = 3), respectively. Determination of As(III) in real water samples yielded satisfactory results.

Keywords: pyridine; carboxylated multiwalled carbon nanotubes; gold nanoparticles; gold staining; linear sweep anodic stripping voltammetry; As(III) analysis



Citation: Du, Y.; Sun, C.; Shen, Y.; Liu, L.; Chen, M.; Xie, Q.; Xiao, H. Anodic Stripping Voltammetric Analysis of Trace Arsenic(III) on a Au-Stained Au Nanoparticles/Pyridine/Carboxylated Multiwalled Carbon Nanotubes/Glassy Carbon Electrode. *Nanomaterials* **2022**, *12*, 1450. <https://doi.org/10.3390/nano12091450>

Academic Editor: Rodolphe Antoine

Received: 13 March 2022

Accepted: 19 April 2022

Published: 24 April 2022

Publisher's Note: MDPI stays neutral with regard to jurisdictional claims in published maps and institutional affiliations.



Copyright: © 2022 by the authors. Licensee MDPI, Basel, Switzerland. This article is an open access article distributed under the terms and conditions of the Creative Commons Attribution (CC BY) license (<https://creativecommons.org/licenses/by/4.0/>).

1. Introduction

Arsenic is widely distributed in the environment and poses a threat to human health [1–4]. Among inorganic arsenic compounds, As(III) has a higher toxicity than As(V) [5,6]. According to the guidelines issued by the World Health Organization, the amount of arsenic should not be higher than 10 ppb in drinking water. On the other hand, an ultralow dose of arsenic trioxide, also known as a Chinese traditional medicine, can well treat acute promyelocytic leukemia [7]. Therefore, the rapid and sensitive detection of As(III) is interesting and important. To date, the analytical methods for arsenic detection mainly include inductively coupled plasma mass spectrometry (ICP-MS) [8], atomic absorption spectrometry (AAS) [8], atomic fluorescence spectrometry (AFS) [8], fluorescent probe method [9,10], biosensing [11], and electroanalysis [12], each with its own characteristics.

The electroanalysis methods, especially anodic stripping voltammetry (ASV), have the advantages of being low cost and using portable instruments, making them appropriate for the rapid and in-field detection of arsenic [13–16]. The ASV analysis of As(III) involves three steps: (1) preconcentration of As(0) under solution-stirred conditions by cathodic potentiostatic reduction of As(III); (2) ceasing solution-stirring to achieve minimum mass

transfer in the bulk solution and minimum potentiostatic electrolysis from the stationary bulk solution; and (3) oxidation of As(0) to As(III) and then to As(V) by an anodic potential sweep. Usually, Au electrodes and Pt electrodes, as well as their modified forms, are used for the ASV analysis of As(III) [13]. Pt has a rather strong affinity for As(0) [17–20], and thus the anodic stripping of As(0) is somewhat difficult on a Pt electrode, making the ASV peak current rather low and the current peak rather broad. In contrast, as Au has an appropriate affinity for As(0), the anodic stripping of As(0) is easy and gives a high ASV peak current and a sharp current peak on a Au electrode, and thus the Au electrode is more favorable for the sensitive analysis of As(III). The Au-involved chemically modified electrodes, e.g., the electrodes modified with gold nanoparticles (AuNPs) [21,22] or their composites with metal oxides [23], silicon materials [24], carbon materials [25,26], and appropriate organic ligands [27–29], can further improve the arsenic analysis performance, either by stabilizing the modified Au material or increasing the effective area of exposed Au surfaces. The pyridine-like organics can act as excellent gold ligands to support and stabilize AuNPs [30,31] and may be developed as new materials for high-performance Au-based arsenic analysis.

Herein, we report the preparation of a Au-stained Au nanoparticle (Au_s)/pyridine (Py)/carboxylated multiwalled carbon nanotubes (C-MWCNTs)/glassy carbon electrode (GCE) by cast-coating of C-MWCNTs on a GCE, electroreduction of 4-cyanopyridine (cPy) to Py, adsorption of gold nanoparticles (AuNPs), and gold staining. The use of 4-cyanopyridine (Py) can lead to the cleavage of the C-C bond between the pyridyl and the cyano group when the 4-cyanopyridine undergoes electroreduction on the electrode, resulting in a pyridine radical. The pyridine radicals are highly active and can be covalently bound well onto the surface of C-MWCNTs/GCE to form Py/C-MWCNTs/GCE. The Py/C-MWCNTs/GCE can provide a good substrate for AuNPs loading and gold staining to increase the Au surface area. Under optimized conditions, the Au_s /Py/C-MWCNTs/GCE can be used for the ASV analysis of As(III), with high sensitivity, low detection limit, high selectivity, good stability, and reproducibility.

2. Experimental Section

2.1. Instrumentation and Reagents

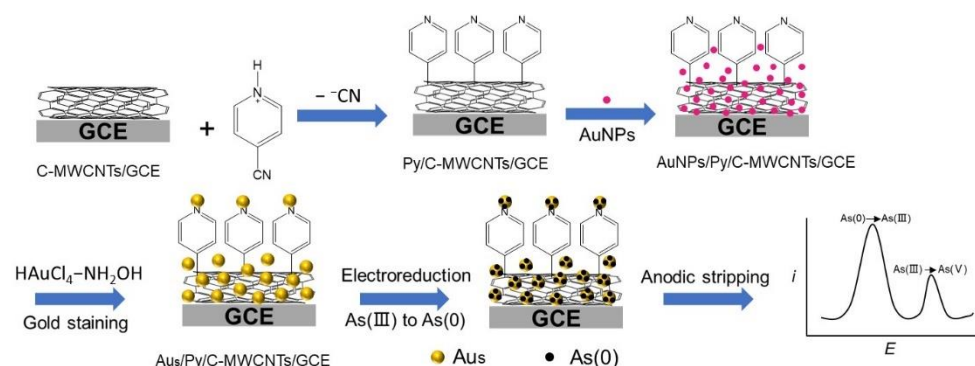
Electrochemical measurements were performed on a CHI660E electrochemical workstation with a three-electrode system. A disk GCE (3.0 mm diameter, 0.0707 cm² geometric area) and its modified electrodes served as the working electrode, a KCl-saturated calomel electrode (SCE) served as the reference electrode, and a platinum wire served as the auxiliary electrode. All potentials are reported versus SCE. A PHS-3C pH meter (Leici, Shanghai, China) was used for pH measurements. The surface plasmon resonance absorption spectra of AuNPs were collected on a UV-visible spectrometer (UV-2450, Shimadzu, Japan). X-ray photoelectron spectroscopy (XPS) data were collected on a Thermo ESCALAB 250XI. A field emission scanning electron microscope (MIRA3 LMH, TESCAN) was used to acquire scanning electron microscopy (SEM) images, and it was equipped with a MAX20 energy-dispersive X-ray spectroscopy (EDX) system for elemental analysis.

4-Cyanopyridine, As(III) stock solution, and $HAuCl_4 \cdot 3H_2O$ were commercially obtained from J&K Scientific (Nanjing, China). Carboxylated multiwalled carbon nanotubes were commercially obtained from XFNANO, Inc. (Nanjing, China). Anhydrous ethanol, $K_4Fe(CN)_6 \cdot 3H_2O$, K_2SO_4 , trisodium citrate, and $CuSO_4 \cdot 5H_2O$ were commercially obtained from Chemicals Company of Tianjin (Tianjin, China). All chemicals are of analytical grade or higher quality. A stock solution of 1.0 mM As(III) in 0.5 M aqueous H_2SO_4 was prepared and stored in a refrigerator at 4 °C, and a series of As(III) standard solutions at the desired concentrations were prepared for immediate use by diluting this As(III) stock solution with 0.5 M aqueous H_2SO_4 . Milli-Q ultrapure water (Millipore, $\geq 18 M\Omega$ cm, USA) was used throughout. The experiments were conducted at room temperature (ca. 25 °C).

2.2. Preparation of $Au_s/Py/C-MWCNTs/GCE$

The bare GCE, after being physically polished, chemically cleaned, and electrochemically cleaned, was characterized in 0.1 M K_2SO_4 solution containing 2.0 mM $K_4[Fe(CN)_6]$ to ensure the high electrode activity.

The cleaned GCE was cast-coated with 6 μ L of 0.2 mg/mL C-MWCNTs dispersion and air-dried to obtain C-MWCNTs/GCE. The C-MWCNTs/GCE was then placed in 0.1 M aqueous H_2SO_4 containing 10 mM 4-cyanopyridine (cPy) and subjected to cyclic voltammetry (CV) treatment for 3 cycles ($-1.2 \sim -0.5$ V, 0.1 V s^{-1}) to obtain Py/C-MWCNTs/GCE. After being water-rinsed and air-dried, the Py/C-MWCNTs/GCE was cast-coated with 10 μ L of AuNPs dispersion for 20 min, washed with ultrapure water, and dried with N_2 to obtain AuNPs/Py/C-MWCNTs/GCE. The AuNPs/Py/C-MWCNTs/GCE was again cast-coated with 10 μ L of gold staining solution (3 mM $HAuCl_4 + 18$ mM $NH_2OH \cdot HCl$) and, after standing for 5 min, washed with ultrapure water to obtain $Au_s/Py/C-MWCNTs/GCE$. The electrode preparation is shown in Scheme 1.



Scheme 1. The preparation of $Au_s/Py/C-MWCNTs/GCE$ for As(III) analysis.

2.3. Electroanalysis of Arsenic(III)

As(III) was detected by linear sweep anodic stripping voltammetry (LSASV). The working electrode was immersed in a stirred 0.1 M aqueous H_2SO_4 containing As(III) at a desired concentration to enrich As(0) at -0.40 V for 420 s. The solution-stirring was then stopped for 15 s, and then the linear sweep anodic stripping of As(0) at 5 V s^{-1} was conducted from -0.40 V to 1.15 V.

3. Results and Discussion

3.1. Preparation and Characterization of $Au_s/Py/C-MWCNTs/GCE$

The AuNPs were prepared according to Ji et al. [32]. The UV-Vis absorption spectrum shows a surface plasmon resonance absorption peak of AuNPs at 521 nm, as shown in Figure S1. The electroreduction of cPy at different pH values was investigated by CV. As shown in Figure 1, 10 mM cPy showed irreversible electroreduction signals at pH 1.0, 3.0, 7.0, 11.0, and 13.0. With the increase in solution pH, the reduction peak shifted negatively and the intensity was weakened. Almost no reduction peak was found in the alkaline environment in the examined potential range. Hence, the electroreduction reaction of cPy was an electron transfer reaction coupled with proton transfer [33,34]. Finally, 0.1 M aqueous H_2SO_4 was selected to dissolve cPy for its electroreduction. As shown in Figure 1B, the irreversible reduction peak at ca. -0.8 V resulted from the reduction of cPy [35]. The electroreduction of cPy will reach saturation in a short time, forming a saturated thin layer structure. In the electrode preparation, the number of cPy-electroreduction cycles was selected to be 3.

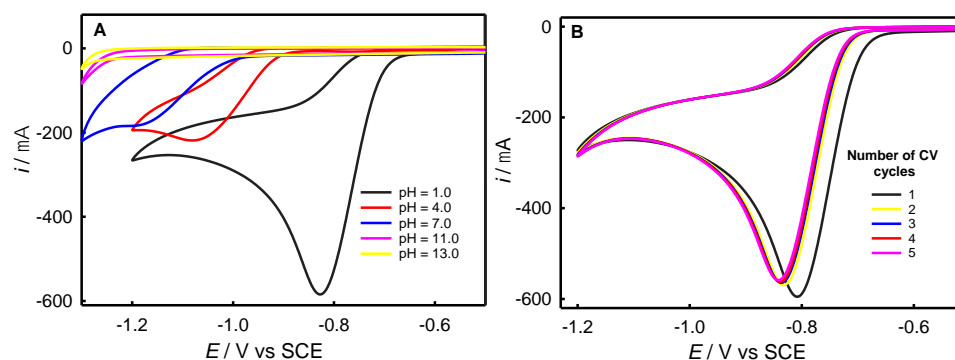


Figure 1. (A) CV curves of 10 mM cPy on GCE at different pH values. (B) CV curves of 0.1 M aqueous H_2SO_4 containing 10 mM cPy on C-MWCNTs/GCE.

C-MWCNTs/GCE and Py/C-MWCNTs/GCE were electrochemically characterized with redox probe 1.0 mM $\text{K}_4\text{Fe}(\text{CN})_6$ in 0.1 M phosphate buffer solution (PBS) at pH 7.0, as shown in Figure S2. Compared with GCE, C-MWCNTs/GCE also showed reversible redox peaks, and the peak currents became slightly larger, indicating good electrode activity. The Py/C-MWCNTs/GCE showed a slightly decreased electrochemical activity versus C-MWCNTs/GCE, implying that an electron-insulating thin-layer Py has been bonded to the electrode surface.

The modified materials and electrodes were characterized by XPS, as shown in Figure 2. After the N1s peaks of Py are separated, the peak positions of Py N and cyano N are at 399.0 eV and 399.8 eV, respectively. When the atoms in the ligand are coordinated or protonated, the density of the electron cloud decreases to a certain extent, which is reflected in the positive shift of the peak position in the XPS spectrum [36,37]. The N1s peak positions of Py and protonated N are at 399.9 eV and 401.9 eV, respectively, and both peaks have a certain degree of positive shift, indicating that the Py ligand was successfully modified on the C-MWCNTs/GCE. Obvious Au 4f peaks are found in Figure 2A,D, indicating that the $\text{Au}_s/\text{Py}/\text{C-MWCNTs}/\text{GCE}$ has been successfully prepared.

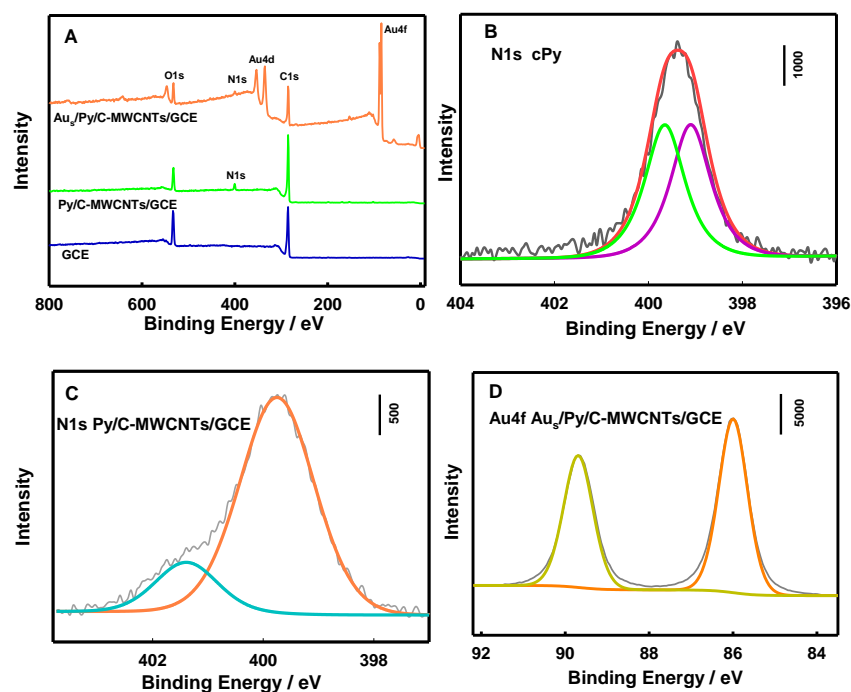


Figure 2. (A) XPS survey of GCE, Py/C-MWCNTs/GCE, and $\text{Au}_s/\text{Py}/\text{C-MWCNTs}/\text{GCE}$; (B) high-resolution N1s region of Py/GCE; (C) high-resolution N1s region of Py/C-MWCNTs/GCE; (D) high-resolution Au4f region of $\text{Au}_s/\text{Py}/\text{C-MWCNTs}/\text{GCE}$.

The $\text{Au}_s/\text{Py}/\text{C-MWCNTs}/\text{GCE}$ was characterized by CV in 0.1 M aqueous H_2SO_4 , as shown in Figure 3. The anodic peaks of ca. 1.1 V and 1.5 V are assigned to the formation peaks of gold oxides (AuO_x). The cathodic peaks of ca. 0 V and 0.9 V are assigned to the reduction peaks of H^+ and AuO_x , respectively. As shown in Figure S3, with the increase in the gold-staining time, the current intensity of the reduction peak of AuO_x increased significantly, and the increase slowed down after the time exceeded 5 min. Therefore, the gold-staining time of 5 min was used in the subsequent experiments. The real surface area of Au (S_{Au}) is positively correlated with the charge of the reduction peak of AuO_x (Q_{AuO_x}) [38] and can be estimated using a conversion factor of $390 \mu\text{C cm}^{-2}$. The ratio of S_{Au} to the geometrical area of the electrode (0.0707 cm^2) gives the roughness factor (R_f). Next, the effect of the time of gold dyeing on the roughness R_f was investigated. Reduction peaks of AuO_x were observed for Au/GCE , $\text{Au}_s/\text{C-MWCNTs}/\text{GCE}$, $\text{Au}_s/\text{Py}/\text{GCE}$, and $\text{Au}_s/\text{Py}/\text{C-MWCNTs}/\text{GCE}$, but the heights of reduction peaks are obviously different. The Q_{AuO_x} of $\text{Au}_s/\text{Py}/\text{C-MWCNTs}/\text{GCE}$ is $58.2 \mu\text{C}$, corresponding to $S_{\text{Au}} = 0.149 \text{ cm}^2$ and $R_f = 2.12$, which are significantly higher than those of Au/GCE , $\text{Au}_s/\text{C-MWCNTs}/\text{GCE}$, and $\text{Au}_s/\text{Py}/\text{GCE}$, indicating that gold staining is a simple and effective method to increase R_f .

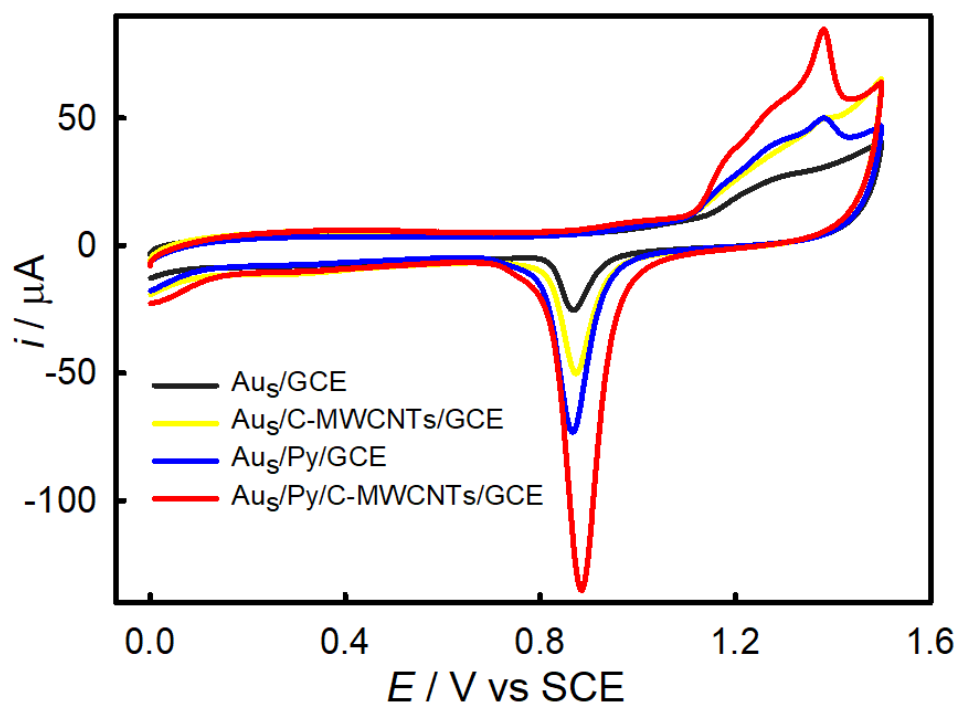


Figure 3. CV curves of Au/GCE , $\text{Au}_s/\text{C-MWCNTs}/\text{GCE}$, $\text{Au}_s/\text{Py}/\text{GCE}$, and $\text{Au}_s/\text{Py}/\text{C-MWCNTs}/\text{GCE}$ (5 min gold staining) in 0.1 M aqueous H_2SO_4 . Scan rate: 50 mV s^{-1} .

The modified electrodes were characterized by SEM and EDX, as shown in Figure 4. The Py/GCE shows a rather smooth surface. The $\text{Py}/\text{C-MWCNTs}/\text{GCE}$ shows random stacking of obvious nanotubes (C-MWCNTs). The $\text{AuNPs}/\text{Py}/\text{C-MWCNTs}/\text{GCE}$ shows obvious and uniform distribution of AuNPs on the GCE substrate and C-MWCNTs. The $\text{AuNPs}/\text{Py}/\text{C-MWCNTs}/\text{GCE}$ shows an increased size and number of Au_s . N and Au elements are found on the $\text{AuNPs}/\text{Py}/\text{C-MWCNTs}/\text{GCE}$, the amount of Au is increased after gold staining.

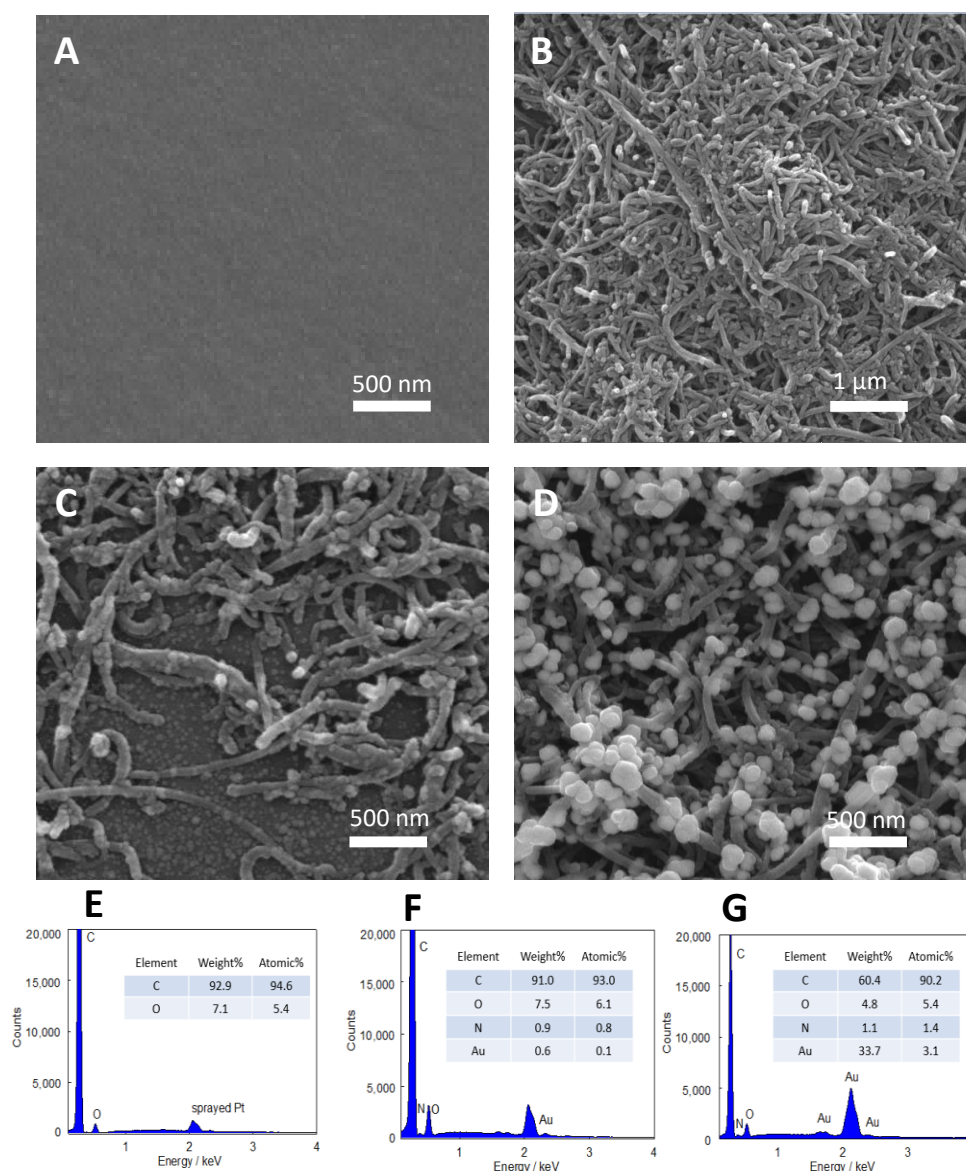


Figure 4. SEM images and EDX spectra of Py/GCE (A,E), Py/C-MWCNTs/GCE (B), AuNPs/Py/C-MWCNTs/GCE (C,F), and Au_s/Py/C-MWCNTs/GCE (D,G).

3.2. LSASV Analysis of As(III)

First, the response of Au_s/Py/C-MWCNTs/GCE to As(III) was investigated by CV and LSASV. Only the reduction peak of AuO_x was observed in the solution without As(III) (red line), as shown in Figure 5A. When As(III) was added to the solution (blue line), Au_s/Py/C-MWCNTs/GCE exhibited characteristic oxidation peaks at 0.25 V and 1.00 V, which are assigned to the electrooxidation of As(0) to As(III) and then to As(V), respectively. The oxidation peak of ca. 1.10 V is due to the oxidation of Au(0) and probably H₂O. The reduction peaks of AuO_x are not very different whether or not As(III) is present, indicating that the enrichment and dissolution of As(0) have little effect on the interface, which also endows the electrode with the ability of continuous detection. The analytical performance comparison of Au/GCE, Au_s/C-MWCNTs/GCE, Au_s/Py/GCE, and Au_s/Py/C-MWCNTs/GCE for As(III) is shown in Figure 5B. Au_s/Py/C-MWCNTs/GCE showed the highest ASV peaks of As(0) to As(III) and As(III) to As(V), and the peak shapes are also good. The Au_s/Py/C-MWCNTs/GCE has the largest R_f value of Au, the highest enriched As(0) efficiency, and the highest analytical sensitivity, due to the largest surface area of Au on this electrode. In addition, the Au film is more stable due to the introduc-

tion of Py-functionalized C-MWCNTs on the electrode surface, which is beneficial for the stability and reproducibility of the electrode in As(III) electroanalysis.

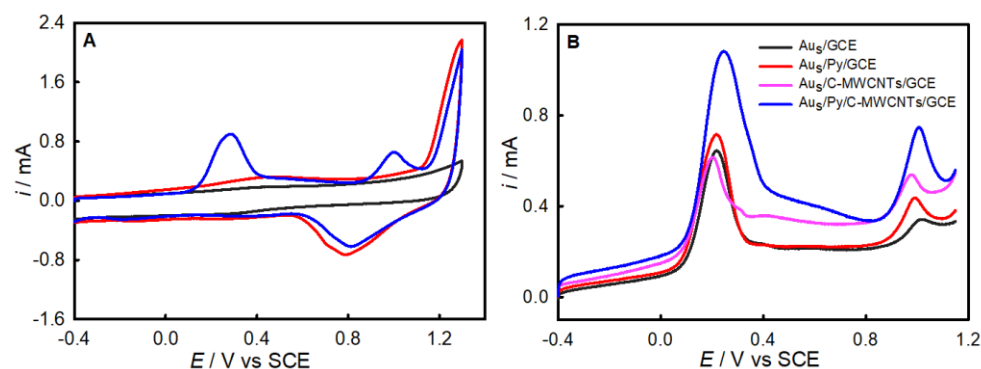


Figure 5. (A) CV curves on GCE (black) and $\text{Au}_5/\text{Py}/\text{C-MWCNTs}/\text{GCE}$ (blue) in 0.1 M aqueous H_2SO_4 containing $1.0 \mu\text{M}$ As(III) and on $\text{Au}_5/\text{Py}/\text{C-MWCNTs}/\text{GCE}$ in As(III)-free 0.1 M aqueous H_2SO_4 (red); (B) LSASV response on the Au-modified electrodes in 0.1 M aqueous H_2SO_4 containing $1.0 \mu\text{M}$ As(III). The experiments were conducted after preconcentration at -0.40 V for 7 min. Scan rate: 5 V s^{-1} .

Subsequently, the conditions for the detection of As(III) by LSASV were optimized. As shown in Figure S4, the dissolution peak heights of As(0) to As(III) and As(III) to As(V) increase with the increase in potential scan rate. However, as the sweep speed increases, the background current and noise also increase. The signal-to-noise ratio (S/N), being the ratio of current (S) to noise (N) at the dissolution peaks of As(0) to As(III) and As(III) to As(V), increases when the potential scan rate is increased. The potential scan rate of 5 V s^{-1} gave the maximum S/N ratio and was thus selected in the subsequent experiments. In addition, a high scan rate can not only save detection time, but also reduce the interference from some kinetically sluggish substances in the solution [39].

The deposition potential (E_D) and deposition time (t_D) were also optimized, as shown in Figures S5 and S6. As shown in Figure S5, the ASV peak heights of As(0) to As(III) and As(III) to As(V) increased as the deposition potential shifted negatively from -0.10 . When the deposition potential reached -0.40 V, the signals of As(0) to As(III) and As(III) to As(V) reached saturation. Therefore, E_D is selected as -0.40 V. As shown in Figure S6, the ASV peaks of As(0) to As(III) and As(III) to As(V) increased with the increase in t_D . When t_D reached 7 min, the signals of As(0) to As(III) and As(III) to As(V) reached saturation. Therefore, t_D is selected as 7 min.

The performance of $\text{Au}_5/\text{Py}/\text{C-MWCNTs}/\text{GCE}$ for the determination of As(III) was investigated under optimal experimental conditions. The continuous LSASV response curves of As(III) at different concentrations and the corresponding standard curves are shown in Figure 6. When the concentration of As(III) in the detection system increases, both the amount of As(0) enriched on the electrode surface and the total force of the interaction between Au and As(0) increase. Hence, the reaction of As(0) to As(III) oxidation requires more energy and gives the slight positive shift of the peak potential. The ASV peak currents of As(0) to As(III) and As(III) to As(V) have a good linear relationship with the concentration of As(III) from 0.01 to $6.00 \mu\text{M}$ ($R^2 = 0.997$) with a sensitivity of $0.741 \text{ mA } \mu\text{M}^{-1}$ and a limit of detection (LOD) of 3.3 nM (0.25 ppb) ($S/N = 3$), and from 0.01 to $6.00 \mu\text{M}$ ($R^2 = 0.991$) with a sensitivity of $0.175 \text{ mA } \mu\text{M}^{-1}$ and an LOD of 16.7 nM (1.20 ppb) ($S/N = 3$), respectively. The comparison of analytical performance in detecting As(III) with reported gold-modified electrodes is listed in Table 1. The $\text{Au}_5/\text{Py}/\text{C-MWCNTs}/\text{GCE}$ gives high sensitivity and a low detection limit, which can meet the requirements for the detection of As(III) in the environment. In addition, it is noteworthy that $\text{Au}_5/\text{Py}/\text{C-MWCNTs}/\text{GCE}$ shows a wide linear concentration range, which is due to the large S_{Au} that makes the enrichment of As(0) not easily reach saturation.

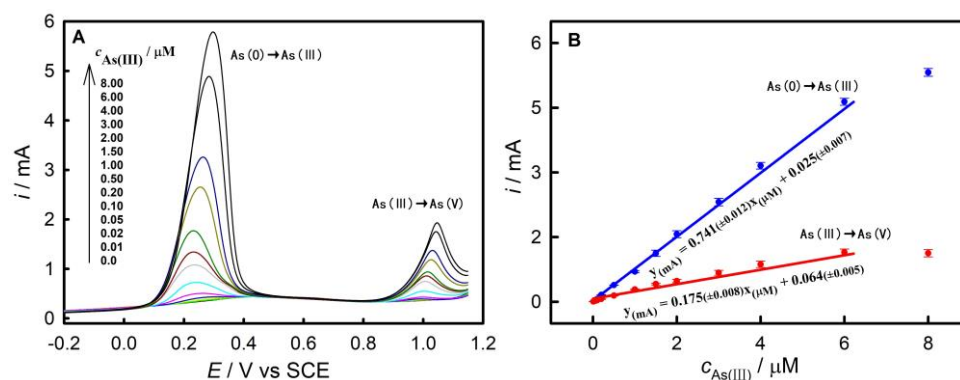


Figure 6. (A) Dual-signal LSASV response on $\text{Au}_s/\text{Py}/\text{C-MWCNTs}/\text{GCE}$ in 0.1 M aqueous H_2SO_4 containing As(III) at different concentrations; (B) the associated calibration curves. $E_D = -0.40$ V, $t_D = 7$ min, scan rate: 5 V s^{-1} .

Table 1. Comparison of the analytical performance of Au and Au-based electrodes for ASV assay of As(III).

Electrode	Technique Used	Oxidation Peak	Sensitivity ($\mu\text{A } \mu\text{M}^{-1}$)	LOD (ppb)	Ref.
AuNPs/ITO	LSV	As(0)→As(III)	58.8	5	[40]
Nano-Au/GCE	LSV	As(0)→As(III)	2.5	1.8	[41]
Au-CNTs/GCE	LSV	As(0)→As(III)	32.5	0.6	[25]
AuNPs-ERGO/GCE	LSV	As(0)→As(III)	12.2	0.2	[42]
Au/Te hybrid/GCE	SWV	As(0)→As(III)	516.2	0.003	[43]
AuNPs/ α - MnO_2 /GCE	SWV	As(0)→As(III)	62.1	0.019	[23]
NF(Au_{nano})/GCE	SWV	As(0)→As(III)	23.4	0.047	[44]
Au-PtNPs/GCE	LSV	As(0)→As(III)	940	0.28	[45]
		As(III)→As(V)	517	0.45	
Au_{temp} /GCE	LSV	As(0)→As(III)	1130	0.495	[46]
		As(III)→As(V)	880	0.654	
$\text{Au}_s/\text{Py}/\text{C-MWCNTs}/\text{GCE}$	LSV	As(0)→As(III)	787	0.25	
		As(III)→As(V)	280	1.20	This work

SWV: square wave anodic stripping voltammetry; AuNPs: gold nanoparticles; ITO: indium tin oxides; ERGO: electroreduced graphene oxide; NF(Au_{nano}): Au-nanoparticle-embedded Nafion; Au_{temp} : porous gold prepared by template removing; CNTs: carbon nanotubes.

The stability and reproducibility of the modified electrodes were investigated. As shown in Figure S7A, for the same $\text{Au}_s/\text{Py}/\text{C-MWCNTs}/\text{GCE}$ electrode performing five consecutive LSASV responses to $1.0 \mu\text{M}$ As(III) solution, the relative standard deviations (RSDs) of As(0) to As(III) and As(III) to As(V) peak currents are 3% and 2%, respectively. As shown in Figure S7B, for the LSASV responses of five $\text{Au}_s/\text{Py}/\text{C-MWCNTs}/\text{GCE}$ electrodes fabricated in the same batch to $1.0 \mu\text{M}$ As(III) solution, the RSDs of As(0) to As(III) and As(III) to As(V) peak currents are 4% and 2%, respectively. After the same $\text{Au}_s/\text{Py}/\text{C-MWCNTs}/\text{GCE}$ electrode was stored in a refrigerator for 7 days, its detection performance was still good, and the ASV peak signal of As(0) to As(III) and As(III) to As(V) still retained 90% performance. The above results indicate that the $\text{Au}_s/\text{Py}/\text{C-MWCNTs}/\text{GCE}$ has good stability and reproducibility.

The interference of Cu^{2+} and As(V) in the system was investigated. In the actual detection process, Cu^{2+} that may exist in the water will form an intermetallic compound [23,43] with the detected target, which will interfere with the detection results of anodic stripping voltammetry. Thus, it is necessary to study the effect of Cu^{2+} on the detection of As(III). As shown in Figure S8, when the Cu^{2+} concentration reaches $1.0 \mu\text{M}$, there is little effect on the dissolution peaks of As(0) to As(III) or As(III) to As(V) in $1.0 \mu\text{M}$ As(III). Therefore, there is no need to worry about the influence of Cu^{2+} in the actual sample detection. Because the deposition potential during detection is -0.40 V, while the reduction deposition of As(V)

requires a more negative potential, so As(V) has little effect on the dissolution peaks of As(0) to As(III) and As(III) to As(V).

Under optimal conditions, analysis of As(III) in actual water samples (tap water, Xiangjiang River water, and Yuelu Mountain spring water) was performed on Au_s/Py/C-MWCNTs/GCE. Analyzed by the standard addition method, the spiked water samples were filtered through a 0.22 μm filter membrane and mixed with an equal volume of 0.2 M H₂SO₄. The results are shown in Table 2. The good recovery values indicate the application potential of the developed electrode for As(III) analysis in actual water samples.

Table 2. Dual-signal LSASV analysis of As(III) in real water samples on Au_s/Py/C-MWCNTs/GCE.

	Determined (μM)	Added (μM)	Found (μM)	Recovery (%)	RSD (%)
Tap water ^a	-	0.100	0.097	97	2.9
Spring water ^a	-	0.100	0.103	103	3.7
River water ^a	0.010	0.100	0.102	102	3.5
Tap water ^b	-	0.100	0.104	104	2.8
Spring water ^b	-	0.100	0.098	98	3.4
River water ^b	0.010	0.100	0.096	96	4.1

^a Detected on Au_s/Py/C-MWCNTs/GCE by the signal of As(0)→As(III) electrooxidation. ^b Detected on Au_s/Py/C-MWCNTs/GCE by the signal of As(III)→As(V) electrooxidation.

4. Conclusions

By cast-coating multiwalled carbon nanotubes on GCE and then modifying pyridine and AuNPs and staining with Au, we have prepared a Au_s/Py/C-MWCNTs/GCE with a high surface area of Au for the sensitive and selective detection of trace As(III). To our knowledge, this is the first example of the combination of pyridine and AuNPs with carbon nanotubes for the detection of As(III), and the combination of carbon materials and organic ligands can improve the loading efficiency of AuNPs for gold staining. In this work, two-step oxidation peaks of As(0)–As(III) and As(III)–As(V) were simultaneously obtained by using fast-speed LSV to achieve the sensitive dual-signal detection of As(III). High analytical performance in the detection of As(III) was obtained. The electrode-preparation strategy may be extended to the field of noble metal electrocatalysis and electrochemical determination of drugs.

Supplementary Materials: The following supporting information can be downloaded at: <https://www.mdpi.com/article/10.3390/nano12091450/s1>. Figure S1. UV-Vis spectrum of the AuNPs; Figure S2. CV curves on GCE, C-MWCNTs/GCE and Py/C-MWCNTs/GCE in 0.1 M PBS containing 1.0 mM K₄Fe(CN)₆ at pH 7.0; Figure S3. CV curves on Au_s/Py/C-MWCNTs/GCE prepared at different gold staining time. Scan rate: 50 mV s⁻¹; Figure S4. (A) CV curves on Au_s/Py/C-MWCNTs/GCE in 0.1 M aqueous H₂SO₄ containing 1.0 μM As(III) at different scan rates, (B) the associated S/N plots of As(0)→As(III) (grey) and As(III)→As(V) (black) vs scan rate, S: peak current, N: noise of the background current. The experiments were conducted after preconcentration at −0.40 V for 7 min; Figure S5. LSASV responses (A) on Au_s/Py/C-MWCNTs/GCE in 0.1 M aqueous H₂SO₄ containing 1.0 μM As(III) at various As(0)-deposition potential (*E*_D) values and the corresponding peak currents versus *E*_D (B). As(0)-deposition time (*t*_D) = 7 min; Figure S6. LSASV responses (A) on Au_s/Py/C-MWCNTs/GCE in 0.1 M aqueous H₂SO₄ containing 1.0 μM As(III) for various As(0)-deposition time (*t*_D) and the corresponding peak currents versus *t*_D (B). *E*_D = −0.40 V; Figure S7. Stability and reproducibility of LSASV response of 1.0 μM As(III). (A) Repeated five times on one Au_s/Py/C-MWCNTs/GCE in 0.1 M aqueous H₂SO₄, (B) On a batch of five different Au_s/Py/C-MWCNTs/GCEs. *E*_D = −0.40 V, *t*_D = 7 min; Figure S8. LSASV response on Au_s/Py/C-MWCNTs/GCE in 0.1 M aqueous H₂SO₄ containing 1.0 μM As(III) with an interval addition of 0.25 μM Cu²⁺. *E*_D = −0.40 V, *t*_D = 7 min.

Author Contributions: Conceptualization, Y.D.; methodology, Y.D.; software, Y.S. and L.L.; resources, Q.X. and H.X.; data curation, C.S. and M.C.; writing—original draft preparation, Y.D.; funding acquisition, Q.X. All authors have read and agreed to the published version of the manuscript.

Funding: This research was supported by the National Natural Science Foundation of China (22074039, 21675050, 22002042).

Conflicts of Interest: The authors declare no conflict of interest.

References

1. Jarup, L. Hazards of heavy metal contamination. *Br. Med. Bull.* **2003**, *68*, 167–182. [[CrossRef](#)] [[PubMed](#)]
2. Shen, S.; Li, X.-F.; Cullen, W.R.; Weinfeld, M.; Le, X.C. Arsenic Binding to Proteins. *Chem. Rev.* **2013**, *113*, 7769–7792. [[CrossRef](#)] [[PubMed](#)]
3. Naujokas, M.F.; Anderson, B.; Ahsan, H.; Aposhian, H.V.; Graziano, J.H.; Thompson, C.; Suk, W.A. The Broad Scope of Health Effects from Chronic Arsenic Exposure: Update on a Worldwide Public Health Problem. *Environ. Health Perspect.* **2013**, *121*, 295–302. [[CrossRef](#)] [[PubMed](#)]
4. Liu, S.X.; Athar, M.; Lippai, I.; Waldren, C.; Hei, T.K. Induction of oxyradicals by arsenic: Implication for mechanism of genotoxicity. *Proc. Natl. Acad. Sci. USA* **2001**, *98*, 1643–1648. [[CrossRef](#)] [[PubMed](#)]
5. Harvey, C.F.; Swartz, C.H.; Badruzzaman, A.B.M.; Keon-Blute, N.; Yu, W.; Ali, M.A.; Jay, J.; Beckie, R.; Niedan, V.; Brabander, D.; et al. Arsenic mobility and groundwater extraction in Bangladesh. *Science* **2002**, *298*, 1602–1606. [[CrossRef](#)] [[PubMed](#)]
6. Wang, Y.; Zhu, G.; Engel, B.; Wu, Y. Probabilistic human health risk assessment of arsenic under uncertainty in drinking water sources in Jiangsu Province, China. *Environ. Geochem. Health* **2020**, *42*, 2023–2037. [[CrossRef](#)]
7. Zhang, X.-W.; Yan, X.-J.; Zhou, Z.-R.; Yang, F.-F.; Wu, Z.-Y.; Sun, H.-B.; Liang, W.-X.; Song, A.-X.; Lallemand-Breitenbach, V.; Jeanne, M.; et al. Arsenic Trioxide Controls the Fate of the PML-RAR alpha Oncoprotein by Directly Binding PML. *Science* **2010**, *328*, 240–243. [[CrossRef](#)] [[PubMed](#)]
8. Leermakers, M.; Baeyens, W.; De Gieter, M.; Smedts, B.; Meert, C.; De Bisschop, H.C.; Morabito, R.; Quevauviller, P. Toxic arsenic compounds in environmental samples: Speciation and validation. *Trac-Trends Anal. Chem.* **2006**, *25*, 1–10. [[CrossRef](#)]
9. Ezech, V.C.; Harrop, T.C. A Sensitive and Selective Fluorescence Sensor for the Detection of Arsenic(III) in Organic Media. *Inorg. Chem.* **2012**, *51*, 1213–1215. [[CrossRef](#)] [[PubMed](#)]
10. Lohar, S.; Sahana, A.; Banerjee, A.; Banik, A.; Mukhopadhyay, S.K.; Matalobos, J.S.; Das, D. Antipyrine Based Arsenate Selective Fluorescent Probe for Living Cell Imaging. *Anal. Chem.* **2013**, *85*, 1778–1783. [[CrossRef](#)] [[PubMed](#)]
11. Kaur, H.; Kumar, R.; Babu, J.N.; Mittal, S. Advances in arsenic biosensor development—A comprehensive review. *Biosens. Bioelectron.* **2015**, *63*, 533–545. [[CrossRef](#)]
12. Luong, J.H.T.; Lam, E.; Male, K.B. Recent advances in electrochemical detection of arsenic in drinking and ground waters. *Anal. Methods* **2014**, *6*, 6157–6169. [[CrossRef](#)]
13. Liu, Z.G.; Huang, X.J. Voltammetric determination of inorganic arsenic. *Trac-Trends Anal. Chem.* **2014**, *60*, 25–35. [[CrossRef](#)]
14. Mays, D.E.; Hussam, A. Voltammetric methods for determination and speciation of inorganic arsenic in the environment—A review. *Anal. Chim. Acta* **2009**, *646*, 6–16. [[CrossRef](#)] [[PubMed](#)]
15. Shin, S.H.; Hong, H.G. Anodic Stripping Voltammetric Detection of Arsenic(III) at Platinum-Iron(III) Nanoparticle Modified Carbon Nanotube on Glassy Carbon Electrode. *Bull. Korean Chem. Soc.* **2010**, *31*, 3077–3083. [[CrossRef](#)]
16. Lan, Y.C.; Luo, H.J.; Ren, X.H.; Wang, Y.P.; Liu, Y.Z. Anodic stripping voltammetric determination of arsenic(III) using a glassy carbon electrode modified with gold-palladium bimetallic nanoparticles. *Microchim. Acta* **2012**, *178*, 153–161. [[CrossRef](#)]
17. Xu, H.; Zeng, L.; Xing, S.; Xian, Y.; Jin, L. Microwave-irradiated synthesized platinum nanoparticles/carbon nanotubes for oxidative determination of trace arsenic(III). *Electrochem. Commun.* **2008**, *10*, 551–554. [[CrossRef](#)]
18. Hrapovic, S.; Liu, Y.; Luong, J.H.T. Reusable platinum nanoparticle modified boron doped diamond microelectrodes for oxidative determination of arsenite. *Anal. Chem.* **2007**, *79*, 500–507. [[CrossRef](#)]
19. Dai, X.; Compton, R.G. Detection of As(III) via oxidation to As(V) using platinum nanoparticle modified glassy carbon electrodes: Arsenic detection without interference from copper. *Analyst* **2006**, *131*, 516–521. [[CrossRef](#)]
20. Xu, H.; Zeng, L.; Xing, S.; Shi, G.; Chen, J.; Man, Y.; Jin, L. Highly ordered platinum-nanotube arrays for oxidative determination of trace arsenic(III). *Electrochem. Commun.* **2008**, *10*, 1893–1896. [[CrossRef](#)]
21. Pu, S.; Sun, H.F.; Hou, X.D.; Xu, K.L. A colorimetric assay for the determination of trace arsenic based on in-situ formation of AuNPs with synergistic effect of arsine and iodide. *Anal. Chim. Acta* **2021**, *1144*, 61–67. [[CrossRef](#)] [[PubMed](#)]
22. Dai, X.; Nekrassova, O.; Hyde, M.E.; Compton, R.G. Anodic stripping voltammetry of arsenic(III) using gold nanoparticle-modified electrodes. *Anal. Chem.* **2004**, *76*, 5924–5929. [[CrossRef](#)] [[PubMed](#)]
23. Yang, M.; Chen, X.; Jiang, T.-J.; Guo, Z.; Liu, J.-H.; Huang, X.-J. Electrochemical Detection of Trace Arsenic(III) by Nanocomposite of Nanorod-like α -MnO₂ Decorated with ~5 nm Au Nanoparticles: Considering the Change of Arsenic Speciation. *Anal. Chem.* **2016**, *88*, 9720–9728. [[CrossRef](#)] [[PubMed](#)]
24. Jena, B.K.; Raj, C.R. Gold nanoelectrode ensembles for the simultaneous electrochemical detection of ultratrace arsenic, mercury, and copper. *Anal. Chem.* **2008**, *80*, 4836–4844. [[CrossRef](#)]
25. Hu, H.B.; Lu, W.J.; Liu, X.N.; Meng, F.C.; Zhu, J.X. A High-Response Electrochemical As(III) Sensor Using Fe₃O₄-rGO Nanocomposite Materials. *Chemosensors* **2021**, *9*, 150. [[CrossRef](#)]
26. Bu, L.J.; Xie, Q.J.; Ming, H. Gold nanoparticles decorated three-dimensional porous graphitic carbon nitrides for sensitive anodic stripping voltammetric analysis of trace arsenic(III). *J. Alloy. Compd.* **2020**, *823*, 153723. [[CrossRef](#)]

27. Farha, F.; Iwamoto, R.T. The Preparation and Infrared Examination of the 2-, 3-, and 4-Cyanopyridine Complexes of Copper(I), Silver(I), and Gold (I) Perchlorates. *Inorg. Chem.* **1965**, *4*, 844–848. [[CrossRef](#)]
28. Yaghi, O.M.; Society, H.L.J.o.t.A.C. T-Shaped Molecular Building Units in the Porous Structure of Ag(4,4'-bpy)-NO₃. *J. Am. Chem. Soc.* **1996**, *118*, 295–296. [[CrossRef](#)]
29. Huang, C.; Zhu, M.; Kang, L.; Dai, B. A novel high-stability Au(III)/Schiff-based catalyst for acetylene hydrochlorination reaction. *Catal. Commun.* **2014**, *54*, 61–65. [[CrossRef](#)]
30. Furukawa, H.; Takahashi, M.; Ito, M. A surface-enhanced Raman study of the electrochemical reduction of 4-cyanopyridine. *Chem. Phys. Lett.* **1986**, *132*, 498–501. [[CrossRef](#)]
31. Shi, C.; Zhang, W.; Birke, R.L.; Lombardi, J.R. SERS investigation of the adsorption and electroreduction of 4-cyanopyridine on a silver electrode. *J. Electroanal. Chem.* **1997**, *423*, 67–81. [[CrossRef](#)]
32. Ji, X.; Song, X.; Li, J.; Bai, Y.; Yang, W.; Peng, X. Size control of gold nanocrystals in citrate reduction: The third role of citrate. *J. Am. Chem. Soc.* **2007**, *129*, 13939–13948. [[CrossRef](#)] [[PubMed](#)]
33. Cole, E.B.; Lakkaraju, P.S.; Rampulla, D.M.; Morris, A.J.; Abelev, E.; Bocarsly, A.B. Using a One-Electron Shuttle for the Multielectron Reduction of CO₂ to Methanol: Kinetic, Mechanistic, and Structural Insights. *J. Am. Chem. Soc.* **2010**, *132*, 11539–11551. [[CrossRef](#)]
34. Yan, Y.; Zeitler, E.L.; Gu, J.; Hu, Y.; Bocarsly, A.B. Electrochemistry of Aqueous Pyridinium: Exploration of a Key Aspect of Electrocatalytic Reduction of CO₂ to Methanol. *J. Am. Chem. Soc.* **2013**, *135*, 14020–14023. [[CrossRef](#)]
35. Xiao, H.; Wang, W.; Pi, S.; Cheng, Y.; Xie, Q. Anodic stripping voltammetry analysis of mercury(II) on a pyridine-Au/pyridine/glassy carbon electrode. *Sens. Actuators B-Chem.* **2020**, *317*, 128202. [[CrossRef](#)]
36. Walton, R.A. The X-ray photoelectron spectra of metal complexes of sulfur-containing ligands: Sulfur 2p binding energies. *Coord. Chem. Rev.* **1980**, *31*, 183–220. [[CrossRef](#)]
37. Morelli, G.; Polzonetti, G.; Sessa, V. Effects of electron density shift in five-coordinated Pt(II) complexes with olefins: An XPS study. *Polyhedron* **1985**, *4*, 1185–1189. [[CrossRef](#)]
38. Trasatti, S.; Petrii, O.A. Real surface area measurements in electrochemistry. *Pure Appl. Chem.* **1991**, *63*, 711–734. [[CrossRef](#)]
39. Bu, L.; Gu, T.; Ma, Y.; Chen, C.; Tan, Y.; Xie, Q.; Yao, S. Enhanced Cathodic Preconcentration of As(0) at Au and Pt Electrodes for Anodic Stripping Voltammetry Analysis of As(III) and As(V). *J. Phys. Chem. C* **2015**, *119*, 11400–11409. [[CrossRef](#)]
40. Dai, X.A.; Compton, R.G. Direct electrodeposition of gold nanoparticles onto indium tin oxide film coated glass: Application to the detection of arsenic(III). *Anal. Sci.* **2006**, *22*, 567–570. [[CrossRef](#)]
41. Hossain, M.M.; Islam, M.M.; Ferdousi, S.; Okajima, T.; Ohsaka, T. Anodic Stripping Voltammetric Detection of Arsenic(III) at Gold Nanoparticle-Modified Glassy Carbon Electrodes Prepared by Electrodeposition in the Presence of Various Additives. *Electroanalysis* **2008**, *20*, 2435–2441. [[CrossRef](#)]
42. Liu, Y.; Huang, Z.; Xie, Q.; Sun, L.; Gu, T.; Li, Z.; Bu, L.; Yao, S.; Tu, X.; Luo, X.; et al. Electrodeposition of electroreduced graphene oxide-Au nanoparticles composite film at glassy carbon electrode for anodic stripping voltammetric analysis of trace arsenic(III). *Sens. Actuators B-Chem.* **2013**, *188*, 894–901. [[CrossRef](#)]
43. Wang, D.; Zhao, Y.; Jin, H.; Zhuang, J.; Zhang, W.; Wang, S.; Wang, J. Synthesis of Au-Decorated Tripod-Shaped Te Hybrids for Applications in the Ultrasensitive Detection of Arsenic. *ACS Appl. Mater. Interfaces* **2013**, *5*, 5733–5740. [[CrossRef](#)]
44. Huang, J.F.; Chen, H.H. Gold-nanoparticle-embedded nafion composite modified on glassy carbon electrode for highly selective detection of arsenic(III). *Talanta* **2013**, *116*, 852–859. [[CrossRef](#)] [[PubMed](#)]
45. Bu, L.J.; Liu, J.; Xie, Q.J.; Yao, S.Z. Anodic stripping voltammetric analysis of trace arsenic(III) enhanced by mild hydrogen-evolution at a bimetallic Au-Pt nanoparticle modified glassy carbon electrode. *Electrochem. Commun.* **2015**, *59*, 28–31. [[CrossRef](#)]
46. Chao, L.; Xiong, X.J.; Liu, J.; Xu, A.G.; Huang, T.; He, F.; Xie, Q.J. Preparation of a porous Au electrode with a sacrificed Prussian blue analogue template for anodic stripping voltammetric analysis of trace arsenic(III). *Sens. Actuators B-Chem.* **2017**, *253*, 603–611. [[CrossRef](#)]